NASA
Technical
Paper
2235

December 1983

Aerodynamic Characteristics, Including Effect of Body Shape, of a Mach 6 Aircraft Concept

Gregory D. Riebe

25th Anniversary
1958-1983

NASA

NASA
Technical
Paper
2235

1983

Aerodynamic Characteristics, Including Effect of Body Shape, of a Mach 6 Aircraft Concept

Gregory D. Riebe

Langley Research Center
Hampton, Virginia

National Aeronautics
and Space Administration

**Scientific and Technical
Information Branch**

1983

SUMMARY

Longitudinal aerodynamic characteristics for a hydrogen-fueled hypersonic transport concept at Mach 6 are presented in this report. The model components consist of four bodies with identical longitudinal area distributions but different cross-sectional shapes and widths, a wing, horizontal and vertical tails, and a set of wing-mounted nacelles simulated by solid bodies on the wing upper surface. Lift-drag ratios were found to be only slightly affected by fuselage planform width or cross-sectional shape. Relative distribution of fuselage volume above and below the wing was found to have an effect on the lift-drag ratio, with a higher lift-drag ratio produced by the higher wing position.

INTRODUCTION

A recent theoretical study (ref. 1) has identified several concepts for hydrogen-fueled cruise aircraft at Mach 6. The study of reference 1 sought to provide conceptual designs which adequately addressed the problem of integrating both ramjet and turbojet propulsion systems with an airframe. One of the propulsion concepts that was selected for experimental analysis featured wing-mounted propulsion systems. This concept consists of high-speed ramjet engines located on the wing lower surface, and turbojet engines, which are required for subsonic-supersonic flight, located directly above on the wing upper surface. The placement of the engines on the wing is advantageous because no boundary-layer diverters are needed for the resulting free-stream inlets.

The study of reference 1, using hypersonic impact theory, showed that a lenticular-shaped fuselage has better lift-drag ratios than a more conventional circular cross-sectional fuselage. Some previous experimental work, at speeds lower than Mach 6, of a configuration with a lenticular fuselage and wing-mounted propulsion systems is discussed in references 2 and 3.

The fuselage of a hydrogen-fueled aircraft would typically be very large because of storage requirements of the low density liquid hydrogen fuel. Trade studies between weight and aerodynamic efficiency for various fuselage cross-sectional shapes would be important for such large fuselages. The scope of the present experimental program was therefore expanded to include not only an investigation of the penalty involved in carrying the turbojet engines during Mach 6 cruise but also of the effect of body cross-sectional shape on overall aerodynamics of the model. Various studies of the relative aerodynamic efficiencies of differently shaped bodies have been made in the past (refs. 4 and 5, for example). The present test was made to see what effect body cross-sectional shape has on the aerodynamics of a representative body-wing configuration at hypersonic speeds. Four different bodies were tested, all having the same longitudinal area distribution but each having a different cross-sectional shape.

The tests were conducted in the Langley 20-Inch Mach 6 Tunnel. Aerodynamic characteristics were obtained at angles of attack from -4° to 8° and at angles of sideslip of 0° and -3°. A theoretical investigation of the model using hypersonic impact theory was also made for comparison with the data.

SYMBOLS

The moment reference point was at a longitudinal station located at 60 percent of the body measured aft from the nose.

A	body cross-sectional area, in^2
a	semi-major axis of ellipse
b	wing span, in.; in table I, semi-minor axis of ellipse
C_D	drag coefficient, Drag/qS
$C_{D,o}$	drag coefficient at zero lift
C_L	lift coefficient, Lift/qS
C_m	pitching-moment coefficient, Pitching moment/qSL
C_n	yawing-moment coefficient, Yawing moment/qSb
C_{n_β}	change of C_n with angle of sideslip, $\frac{C_{n_{\beta=-3^0}} - C_{n_{\beta=0^0}}}{-3}$, deg^{-1}
C_Y	side-force coefficient, Side force/qS
C_{Y_β}	change of C_Y with angle of sideslip, $\frac{C_{Y_{\beta=-3^0}} - C_{Y_{\beta=0^0}}}{-3}$, deg^{-1}
C_l	rolling-moment coefficient, Rolling moment/qSb
C_{l_β}	change of C_l with angle of sideslip, $\frac{C_{l_{\beta=-3^0}} - C_{l_{\beta=0^0}}}{-3}$, deg^{-1}
c	chord
d	diameter, in.
L	body length, 24.00 in.
L/D	lift-drag ratio
q	dynamic pressure, psia
r	cross-sectional radius, in.
S	reference area, in^2
w	width
x	axial distance along body from nose, in.
y	spanwise coordinate from body centerline, in.

y_{max} maximum value of y at particular cross section, in.

z vertical coordinate from reference line, in.

α angle of attack, deg

β angle of sideslip, deg

Subscripts:

l lower

u upper

Model components:

B body

B_1 lenticular-shaped body

B_2 axisymmetric (circular) body

B_3 bielliptical body with width equal to that of B_1 and upper and lower areas equal to those of B_1

B_4 body like B_3 except width equal to average of widths of B_1 and B_2

H horizontal tail, subscript indicates deflection

N nacelle

N_I nacelle in inboard position

N_M nacelle in middle position

N_O nacelle in outboard position

V vertical tail

W wing

APPARATUS AND TESTS

Description of Model

A three-view drawing of the nominal complete configuration is shown in figure 1. A photograph of this configuration in the Langley 20-Inch Mach 6 Tunnel is shown in figure 2. The cross sections of the body shown in these two figures are lenticular. The wing airfoil is a 3-percent-thick wedge-slab-wedge section, with chordwise wedge half-angles of 3° and 4° at the leading and trailing edges, respectively. The nacelle is solid, with no airflow through it, as would be true in Mach 6 flight. The nacelle could be mounted in three different spanwise locations, as shown in the frontal view in figure 1. No ramjets were modeled for this test because the main interest was in the increment in lift-drag ratio caused by the turbojet nacelles which would not be used at Mach 6. The vertical tail has a 12-percent-thick wedge airfoil and the horizontal tails utilize a 6-percent-thick symmetrical diamond airfoil with maximum thickness at 50 percent chord.

Three other bodies were also tested, all having the same longitudinal area distribution as the first. The relative shapes of the four body cross sections are shown in figure 3. At the top of the figure is B_1 which is lenticular. Body B_2 is an axisymmetric (circular) body. Body B_3 is bielliptical, with a width equal to that of B_1 and upper and lower areas equal to those of B_1. Body B_4 is like B_3 except that the width of B_4 is equal to the average of the widths of B_1 and B_2. Figure 4 shows the planform and profile shapes of the four bodies. All four bodies had various amounts of camber because no attempt to match body camber was made. A plot of the longitudinal area distribution of the bodies is found in figure 5.

A detailed geometric description of each body can be found in table I; geometric characteristics of the model components are listed in table II. Notice in table II that there are three different reference spans and reference areas. For this test, the exposed wing area was kept constant; thus, the reference spans and areas change with body width. For all bodies, the wing reference plane coincides with the body reference plane.

Wind Tunnel and Test Conditions

The investigation was conducted in the Langley 20-Inch Mach 6 Tunnel, which is a blowdown-type wind tunnel that exhausts into the atmosphere or vacuum spheres. The tunnel has a two-dimensional nozzle and a test section 20.5 in. high and 20.0 in. wide. A more detailed description of this tunnel can be found in reference 6.

The tests were conducted at Mach 6 and at a nominal stagnation pressure and temperature of 400 psi and 900°R, respectively. The corresponding free-stream Reynolds number per foot was 6.56×10^6. Aerodynamic force and moment data were obtained over a range of angle of attack from -4° to 8° and at angles of sideslip of 0° and -3°. Horizontal tail deflections include 0°, -10°, and -20°. No attempt was made to trip the boundary layer.

Data Acquisition and Reduction

Aerodynamic force and moment data were measured with a six-component strain-gauge balance which was housed inside the model body and attached to the tunnel sting support system. The movable sting support system was pneumatically driven through the angle-of-attack range during each run. The angles of attack and sideslip were set optically by using a prism mounted on the model to reflect a point source of light onto a calibrated chart. The Mach number was obtained with a total-pressure probe which was inserted into the test section upstream of the model at the beginning and end of each run. (Force data were not recorded with the probe in the tunnel.) The Mach number for each test point was then determined by linear interpolation with time. Typical Mach number variation was less than 1 percent.

Straight-line slopes between the data at $\beta = 0°$ and $\beta = -3°$ were used to obtain the lateral-directional stability parameters. Model chamber pressure was determined from the average of two measurements and was used to adjust the axial-force data to correspond to a base pressure equal to free-stream static pressure. Nacelle base pressures were not measured. The reference spans and areas shown in table II were used in calculating the force coefficients for the different configurations.

THEORETICAL METHOD

A theoretical analysis of the model was made using the Spalding-Chi skin-friction calculation method with turbulent flow assumed (ref. 7) and with tangent-cone impact theory on the bodies and tangent-wedge impact theory on the wings (refs. 8 and 9). The numerical representation of the wind-tunnel-model geometry was specified according to the method of reference 10, and additional coding was used to translate the surface geometry to the input format for the computer program of references 8 and 9. A computer-generated three-view drawing along with an oblique-view drawing from the program of reference 10 for the B_1W configuration is shown in figure 6.

DISCUSSION

In figure 7, the static longitudinal aerodynamic characteristics for the B_1 configuration buildup are presented. The trends are as expected: increased C_L with increased planform area; improvement in longitudinal stability with the addition of the wing, with further improvement upon adding the tails; increased $C_{D,o}$ for each added component; a major improvement in maximum L/D with the addition of the wing, then a decrease with each added component. Note that the addition of the nacelles resulted in an 8-percent drop in maximum L/D.

The aerodynamic characteristics of the four bodies alone are compared in figure 8. The wider bodies have higher maximum lift-drag ratios than do the narrower bodies. The positive C_L at $C_m = 0$ for B_1, B_3, and B_4 is caused by the camber of the bodies. A comparison of the theoretical and experimental aerodynamic characteristics of the four bodies alone is presented in figure 9. The tangent-cone theory cannot account for losses due to pressure bleed around the edge of the bodies and possible separation on the upper surface; therefore, a much higher L/D is predicted than is achieved.

With the addition of the wing, the trends found in the data for the bodies alone are changed, as can be seen in figure 10, where the aerodynamic characteristics of the four BW configurations are presented. At positive C_L, L/D for the B_2W configuration is the same as that for the B_1W and B_3W configurations, which was not an expected result because it was thought that using a wider body would result in a higher body-wing L/D. Also seen in the L/D curves is that at negative lift coefficients, the values of L/D are greater in magnitude than those at positive C_L for all configurations except B_2W (maximum L/D was not achieved at negative α because of balance fouling). In other words, these configurations are more aerodynamically efficient when inverted. These results are probably caused by the difference in the distribution of body volume above and below the wing. As mentioned previously, the wing reference plane coincides with the body reference plane. As was seen in figures 4 and 5, bodies 1, 3, and 4 have considerably more volume above the reference plane than below it. This larger volume above the reference plane causes larger interference pressures on the wing upper surface than those occurring on the lower wing surface; thus, lift is reduced. This reasoning is supported by the fact that the curves for C_L versus α for the body-wing configurations show a negative C_L at $\alpha = 0$ for bodies 1, 3, and 4 as compared with $C_L = 0$ at $\alpha = 0$ for the body-alone configurations shown in figure 8. Inverting the configurations (or raising the wing) should put the larger interference pressures on the bottom; thus, L/D is improved. The tangent-wedge estimates for the wings, when added to the tangent-cone estimates of the bodies, are shown in figure 11. This method of calculating forces is unable to predict interactions between components and, therefore, could not take into account the body-generated pressure field acting on the wing.

The effect of nacelle location on lift-drag ratio of the B_1WN configuration is shown in figure 12. Moving the nacelles inboard results in a slight increase in L/D, probably because of a decrease in the amount of wing upper surface influenced by the positive pressure field generated by the nacelles. Nacelles may also produce positive interference effects over the boattailed fuselage areas.

Horizontal tail effectiveness is shown in figure 13. The configuration would be trimmed and neutrally stable for a tail deflection of about -2°. As seen by the curves for C_D and L/D, a small negative horizontal tail deflection would improve the aerodynamics of the complete configuration.

Lateral-directional characteristics are presented in figures 14 and 15. The total configuration is laterally and directionally stable at all angles of attack. (See fig. 14.) Although all body-alone configurations are directionally unstable, the body with the smallest profile area (B_3) is the least directionally unstable. (See fig. 15.)

CONCLUSIONS

Longitudinal aerodynamic characteristics for a hydrogen-fueled hypersonic transport concept at Mach 6 are presented in this report. The model components consisted of four bodies with identical longitudinal area distributions but different cross-sectional shapes and widths, a wing, horizontal and vertical tails, and a set of wing-mounted nacelles simulated by solid bodies mounted on the wing upper surface. The following conclusions can be drawn from this study:

1. Body cross-sectional shape for the range of geometries studied appears to have little impact on body-wing configuration lift-drag ratio which is contrary to impact theory predictions.

2. The relative distribution of fuselage volume above and below the wing has an effect on the aerodynamic efficiency of the body-wing configurations tested.

3. The addition of the nacelles on the wing upper surface of the nominal configuration resulted in an 8-percent drop in maximum lift-drag ratio.
4. For the nominal configuration, a slight increase in lift-drag ratio can be realized by properly placing engine nacelles in close proximity to the fuselage.

Langley Research Center
National Aeronautics and Space Administration
Hampton, VA 23665
November 4, 1983

REFERENCES

1. Morris, R. E.; and Brewer, G. D.: Hypersonic Cruise Aircraft Propulsion Integration Study. NASA CR-158926-2, 1979.

2. Riebe, Gregory D.; and Pittman, Jimmy L.: Aerodynamic Characteristics of a Hypersonic Cruise Aircraft Concept With Wing-Mounted Propulsion Systems at Mach Numbers of 2.96, 3.96, and 4.63. NASA TM X-81937, 1981.

3. Pittman, Jimmy L.; and Riebe, Gregory D.: Experimental and Theoretical Aerodynamic Characteristics of Two Hypersonic Cruise Aircraft Concepts at Mach Numbers of 2.96, 3.96, and 4.63. NASA TP-1767, 1980.

4. Fuller, Dennis E.; Shaw, David S.; and Wassum, Donald L.: Effect of Cross-Section Shape on the Aerodynamic Characteristics of Bodies at Mach Numbers From 2.50 to 4.63. NASA TN D-1620, 1963.

5. Harris, Roy V., Jr.; and Landrum, Emma Jean: Drag Characteristics of a Series of Low-Drag Bodies of Revolution at Mach Numbers From 0.6 to 4.0. NASA TN D-3163, 1965.

6. Keyes, J. Wayne: Force Testing Manual for the Langley 20-Inch Mach 6 Tunnel. NASA TM-74026, 1977.

7. Spalding, D. B.; and Chi, S. W.: The Drag of a Compressible Turbulent Boundary Layer on a Smooth Flat Plate With and Without Heat Transfer. J. Fluid Mech., vol. 18, pt. 1, Jan. 1964, pp. 117-143.

8. Gentry, Arvel E.: Hypersonic Arbitrary-Body Aerodynamic Computer Program (Mark III Version). Volume I - User's Manual. Rep. DAC 61552, Vol. I (Air Force Contract Nos. F33615 67 C 1008 and F33615 67 C 1602), McDonnell Douglas Corp., Apr. 1968. (Available from DTIC as AD 851 811.)

9. Gentry, Arvel E.; and Smyth, Douglas N.: Hypersonic Arbitrary-Body Aerodynamic Computer Program (Mark III Version). Volume II - Program Formulation and Listings. Rep. DAC 61552, Vol. II (Air Force Contract Nos. F33615 67 C 1008 and F33615 67 C 1602), McDonnell Douglas Corp., Apr. 1968. (Available from DTIC as AD 851 812.)

10. Stack, Sharon H.; Edwards, Clyde L. W.; and Small, William J.: GEMPAK: An Arbitrary Aircraft Geometry Generator. NASA TP-1022, 1977.

TABLE I.- GEOMETRIC DESCRIPTION OF MODEL BODIES

Body 1

x, in.	y_{max}, in.	z_u, in.	z_l, in.	r_u, in.	r_l, in.
0	0	0	0	0	0
2	.3286	.3225	-.0581	.3287	-.9583
4	.6183	.5484	-.1162	.6228	-1.7031
6	.8676	.7121	-.1743	.8846	-2.2464
8	1.0735	.8390	-.2325	1.1063	-2.5945
10	1.2278	.9008	-.2906	1.2872	-2.7391
12	1.3064	.9040	-.3487	1.3960	-2.6216
14	1.3193	.8432	-.4068	1.4537	-2.3427
16	1.2708	.7823	-.4510	1.4233	-2.0159
18	1.1330	.7215	-.4657	1.2503	-1.6111
20	.9476	.6606	-.4771	1.0099	-1.1796
22	.7346	.6000	-.4885	.7497	-.7966
24	.5000	.5000	-.5000	.5000	-.5000

Body 2

x, in.	r, in.
0	0
2	.2376
4	.4400
6	.6083
8	.7300
10	.8150
12	.8627
14	.8654
16	.8360
18	.7731
20	.6965
22	.6051
24	.5000

Body 3

x, in.	a, in.	b_u, in.	b_l, in.
0	0	0	0
2	.3286	.3061	-.0514
4	.6183	.5191	-.1028
6	.8676	.6640	-.1542
8	1.0735	.7602	-.2057
10	1.2278	.8161	-.2571
12	1.3064	.8139	-.3085
14	1.3193	.7616	-.3600
16	1.2708	.7093	-.3880
18	1.1330	.6569	-.4160
20	.9476	.6046	-.4440
22	.7346	.5523	-.4720
24	.5000	.5000	-.5000

Body 4

x, in.	a, in.	b_u, in.	b_l, in.
0	0	0	0
2	.2891	.3527	-.0630
4	.5290	.6049	-.1260
6	.7335	.7871	-.1890
8	.8990	.9110	-.2520
10	1.0230	.9852	-.3150
12	1.0794	.9830	-.3780
14	1.0890	.9177	-.4410
16	1.0454	.8470	-.4791
18	.9494	.7724	-.4952
20	.8222	.6946	-.5000
22	.6714	.6140	-.5000
24	.5000	.5000	-.5000

TABLE II.- GEOMETRIC CHARACTERISTICS OF THE WIND-TUNNEL MODEL COMPONENTS

	Body 1	Body 2	Body 3	Body 4
Reference area, in^2	49.14	44.10	49.14	46.56
Reference span, in.	11.24	10.34	11.24	10.78
Aspect ratio	2.57	2.42	2.57	2.50

Body:	
Length, in.	24.00
Volume, in^3	34.79
Wing:	
Root chord at body centerline, in.	5.60
Tip chord, in.	1.223
Taper ratio	0.218
Trailing-edge sweepback angle, deg:	
Inboard panel	35.00
Outboard panel	20.00
Leading-edge sweepback angle, deg:	
Inboard panel	35.00
Outboard panel	60.00
Dihedral angle, deg:	
Inboard panel	0
Outboard panel	2.00
Incidence angle, deg	0
Airfoil thickness ratio	0.03
Leading-edge radius, in.	0.005
Horizontal tail:	
Span, in.	4.50
Root chord at $y = 0.500$, in.	2.81
Tip chord, in.	0.40
Taper ratio	0.156
Trailing-edge sweepback angle, deg	20.00
Leading-edge sweepback angle, deg	60.00
Dihedral angle, deg	0.00
Incidence angle, deg	0.00
Airfoil thickness ratio	0.06
Leading-edge radius, in.	0.005
Vertical tail:	
Maximum height above root chord, in.	2.50
Root chord at $z = 0.500$ in.	3.45
Tip chord, in.	1.18
Taper ratio	0.34
Trailing-edge sweepback angle, deg	27.50
Leading-edge sweepback angle, deg	55.00
Airfoil thickness ratio	0.12
Wedge angle, normal to leading edge, deg	6.00
Leading-edge radius, in.	0.005
Projected base area, in^2	0.695

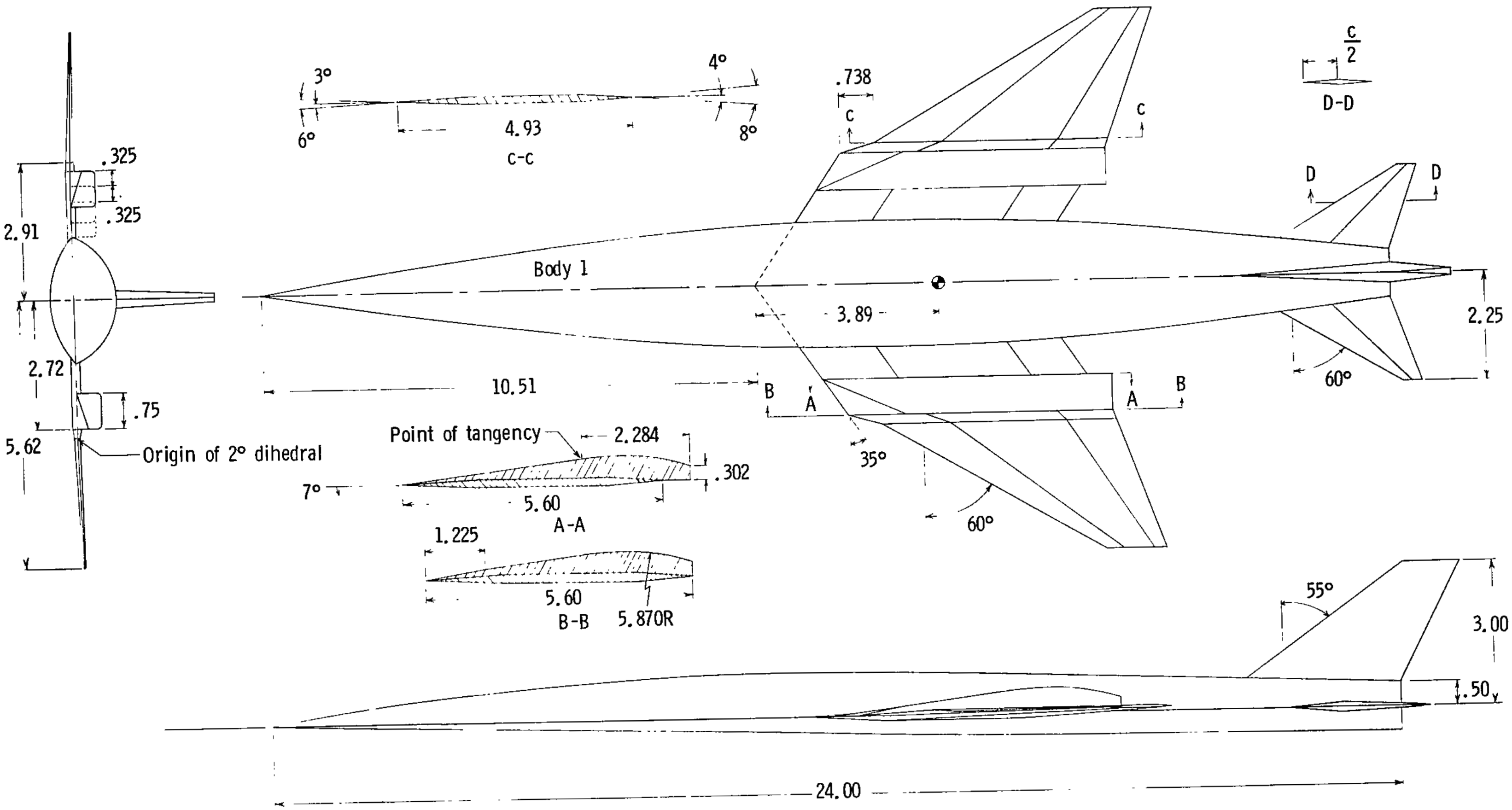

Figure 1.- Drawing of B_1WN_OHV configuration. Linear dimensions are in inches.

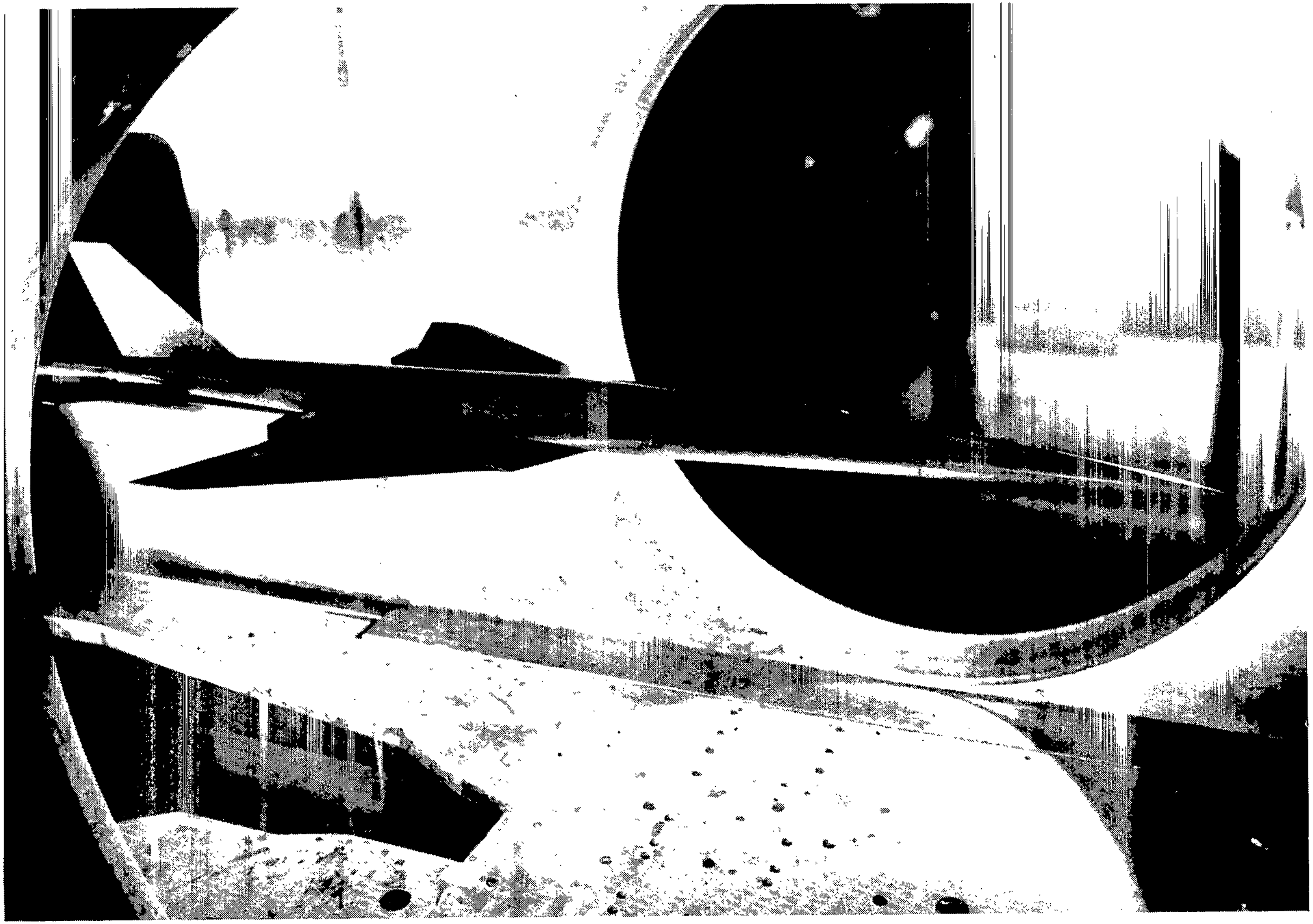

L-80-10,060

Figure 2.- Photograph of B_1WN_0HV configuration in Langley 20-Inch Mach 6 Tunnel.

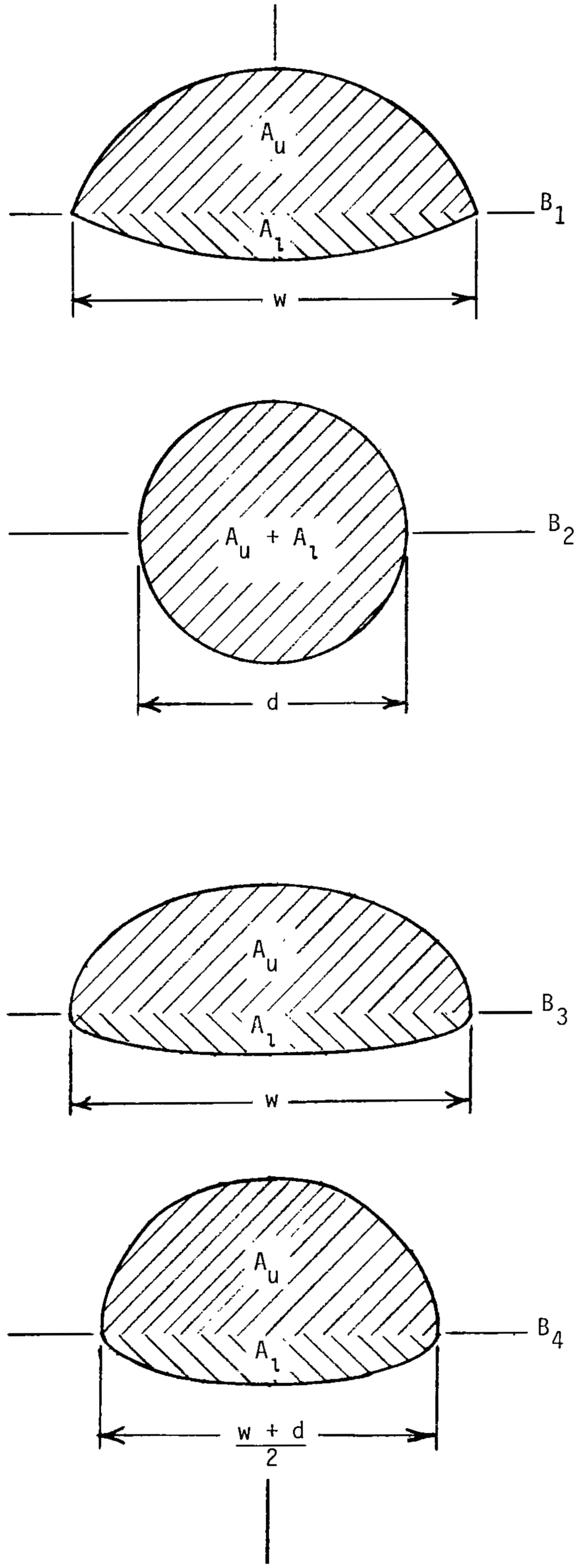

Figure 3.- Cross-sectional shapes of four bodies at location 12 in. behind nose.

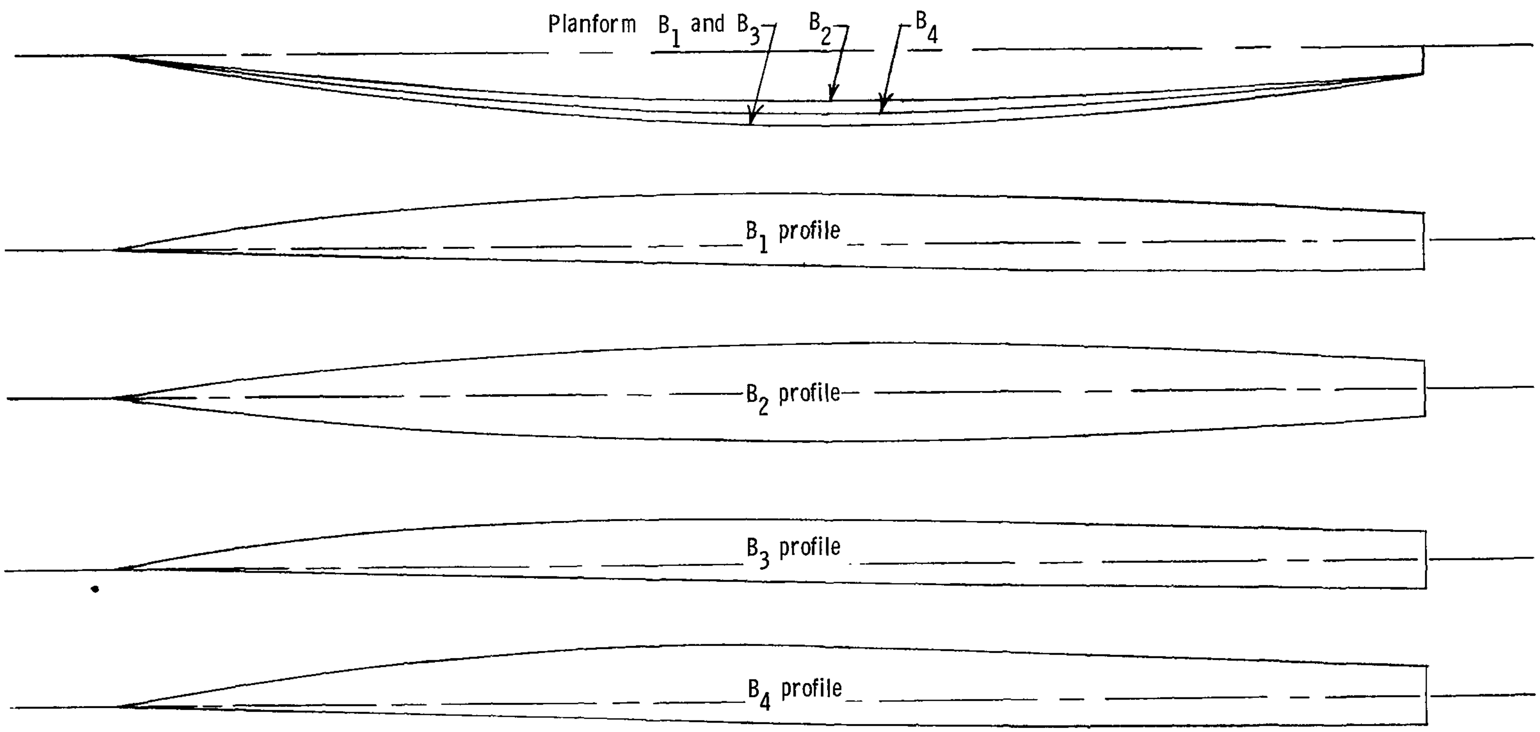

Figure 4.- Comparison of planform and profile shapes of four bodies.

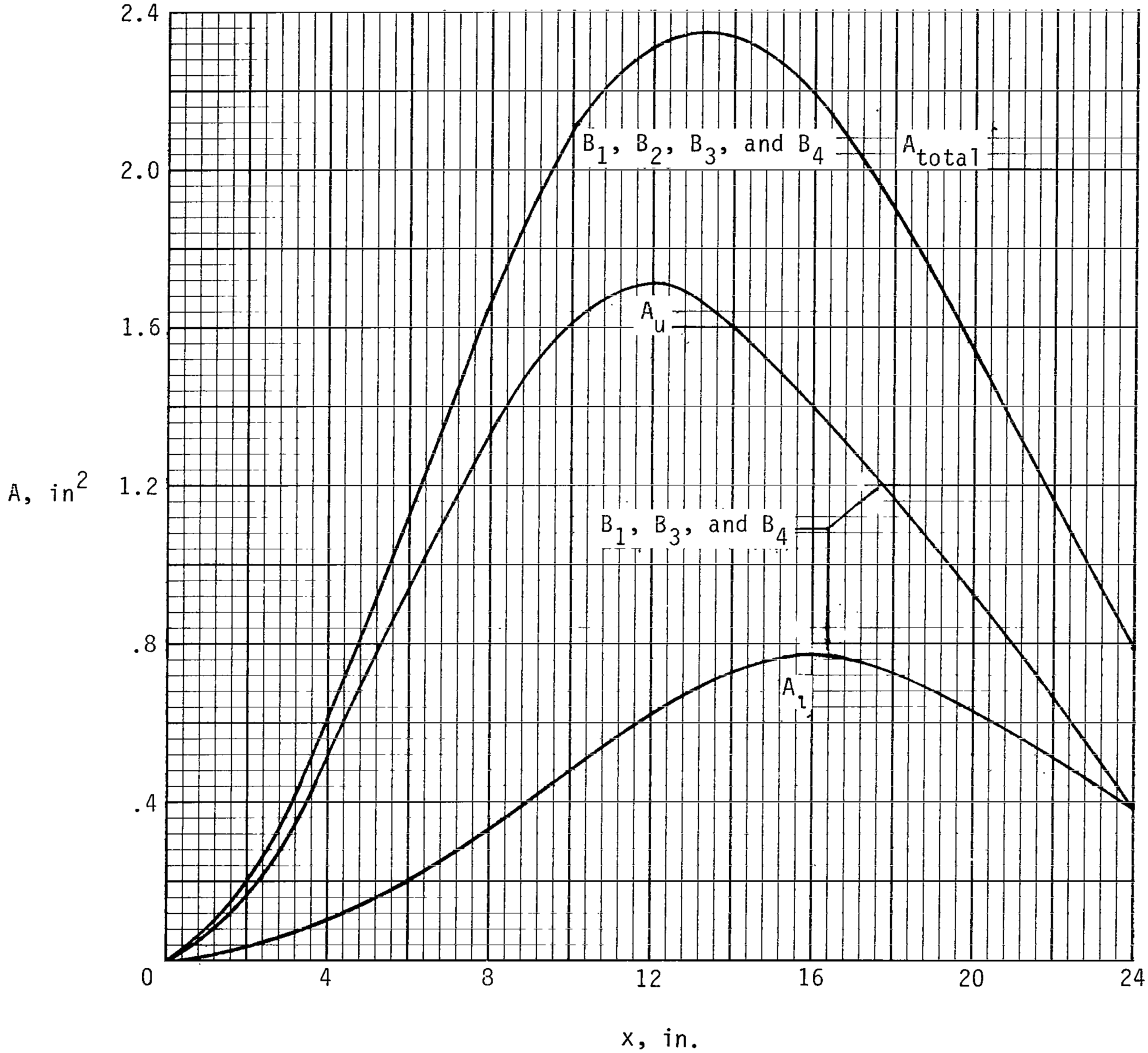

Figure 5.- Area distribution for body-alone configuration.

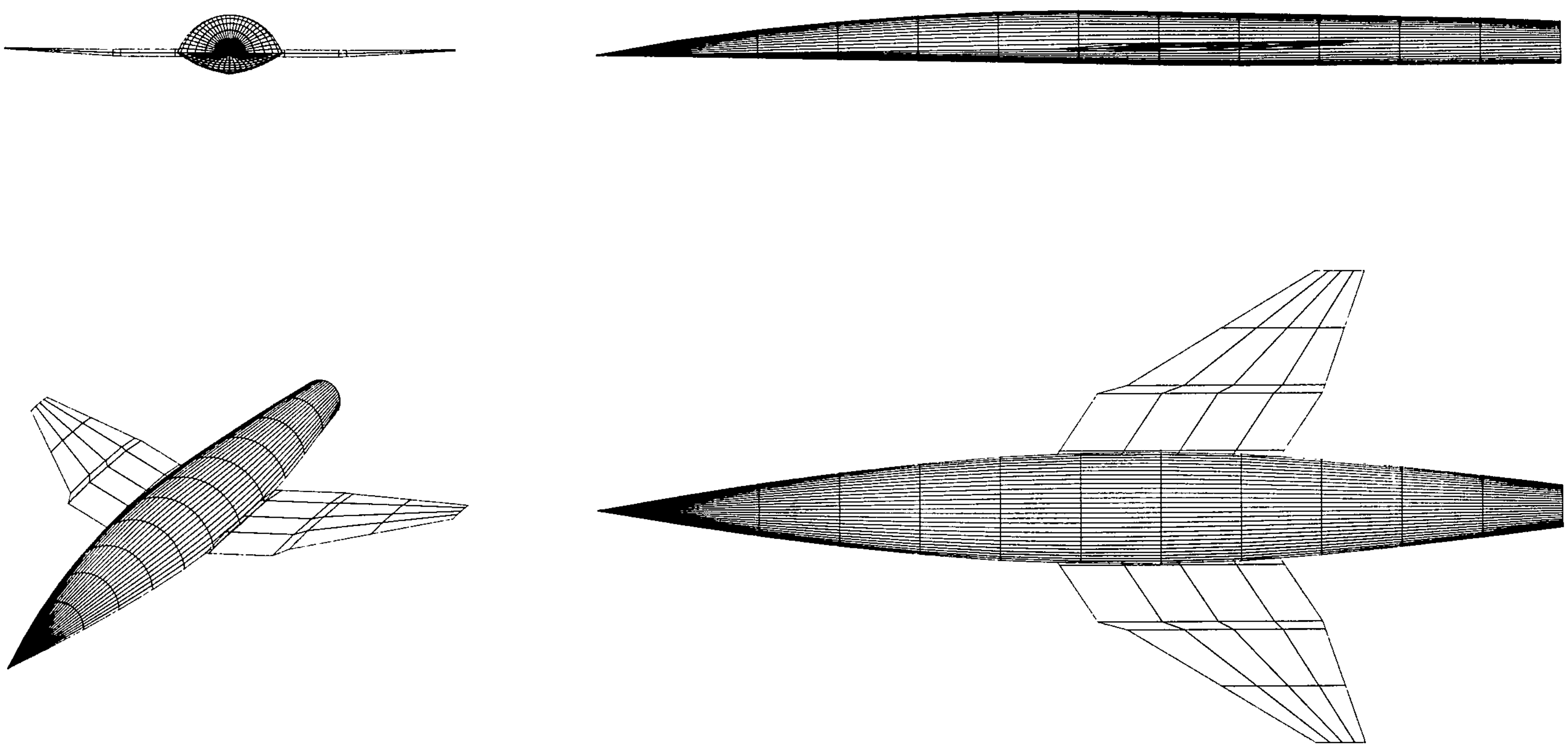

Figure 6.- Computer-generated drawing of B_1W configuration.

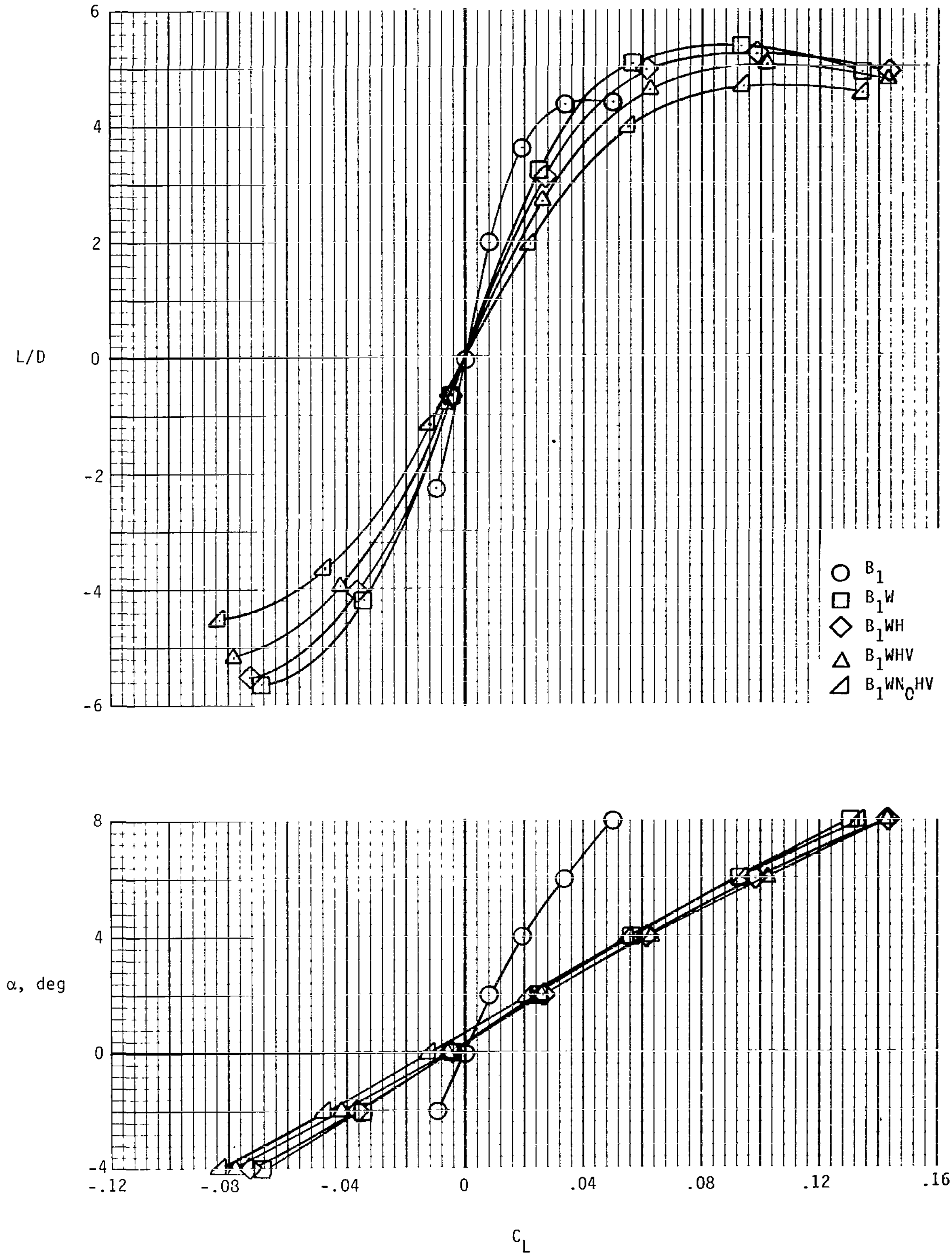

Figure 7.- Longitudinal aerodynamic characteristics for B_1 configuration buildup.

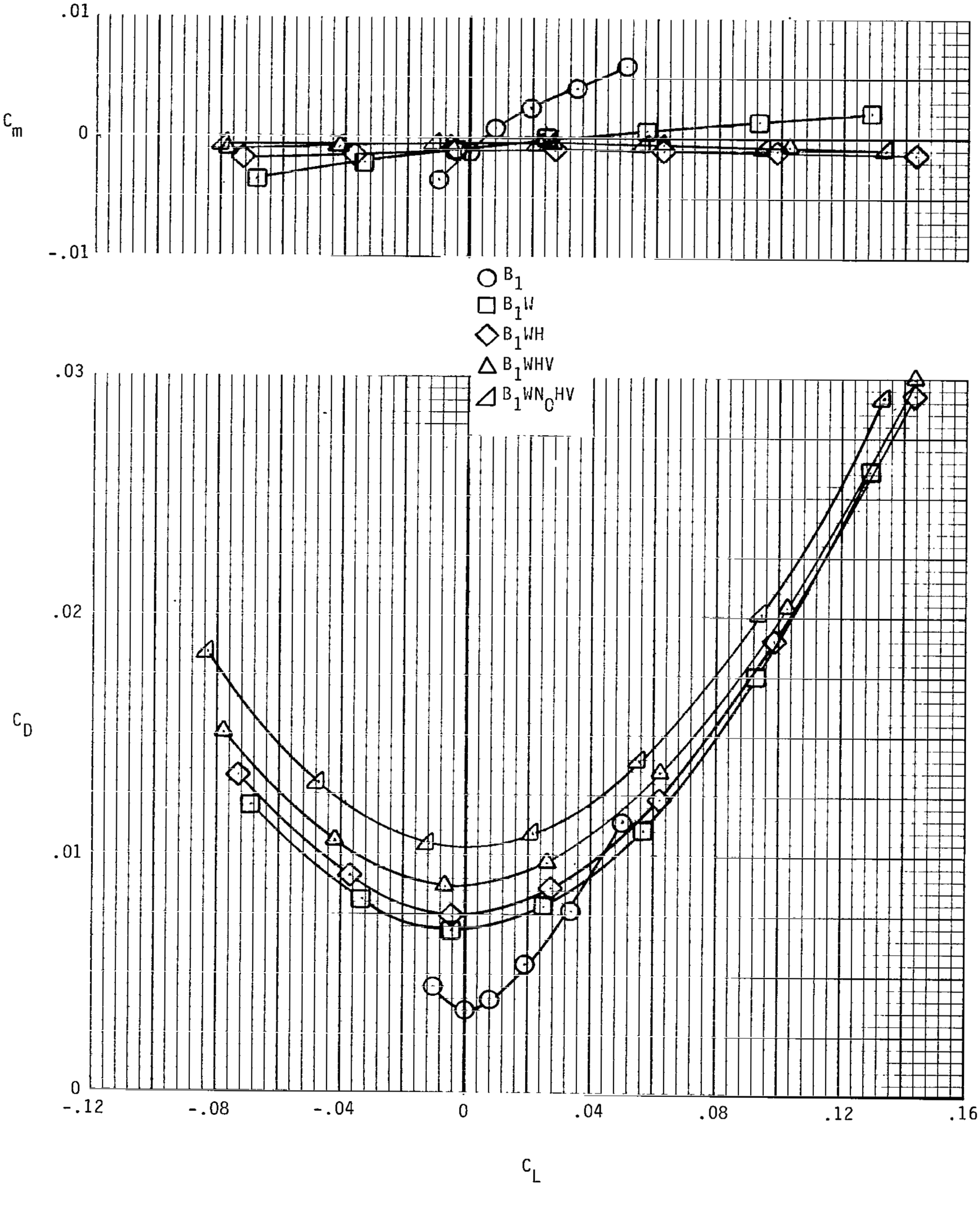

Figure 7.- Concluded.

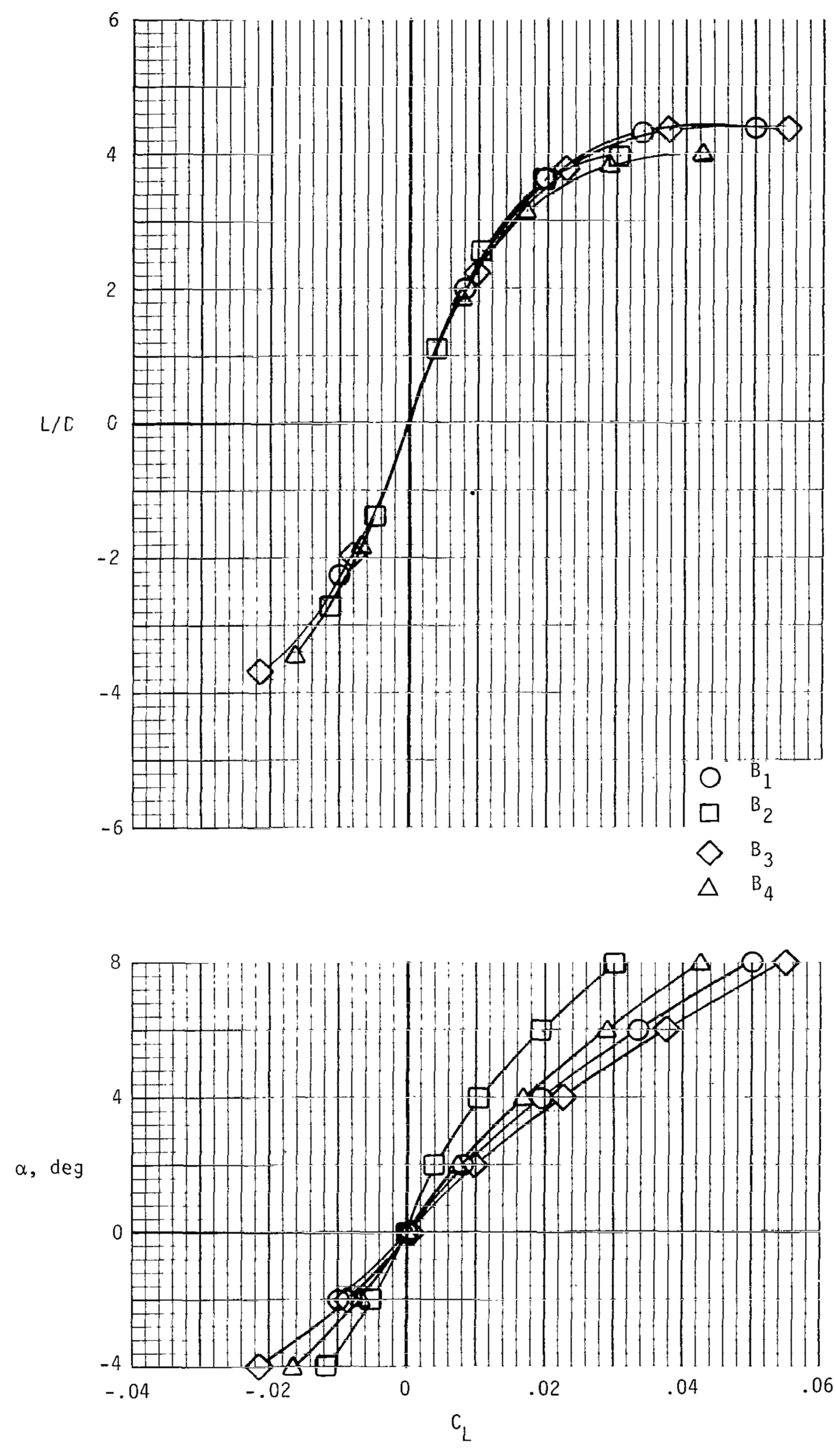

Figure 8.- Comparison of longitudinal aerodynamic characteristics of four body-alone configurations.

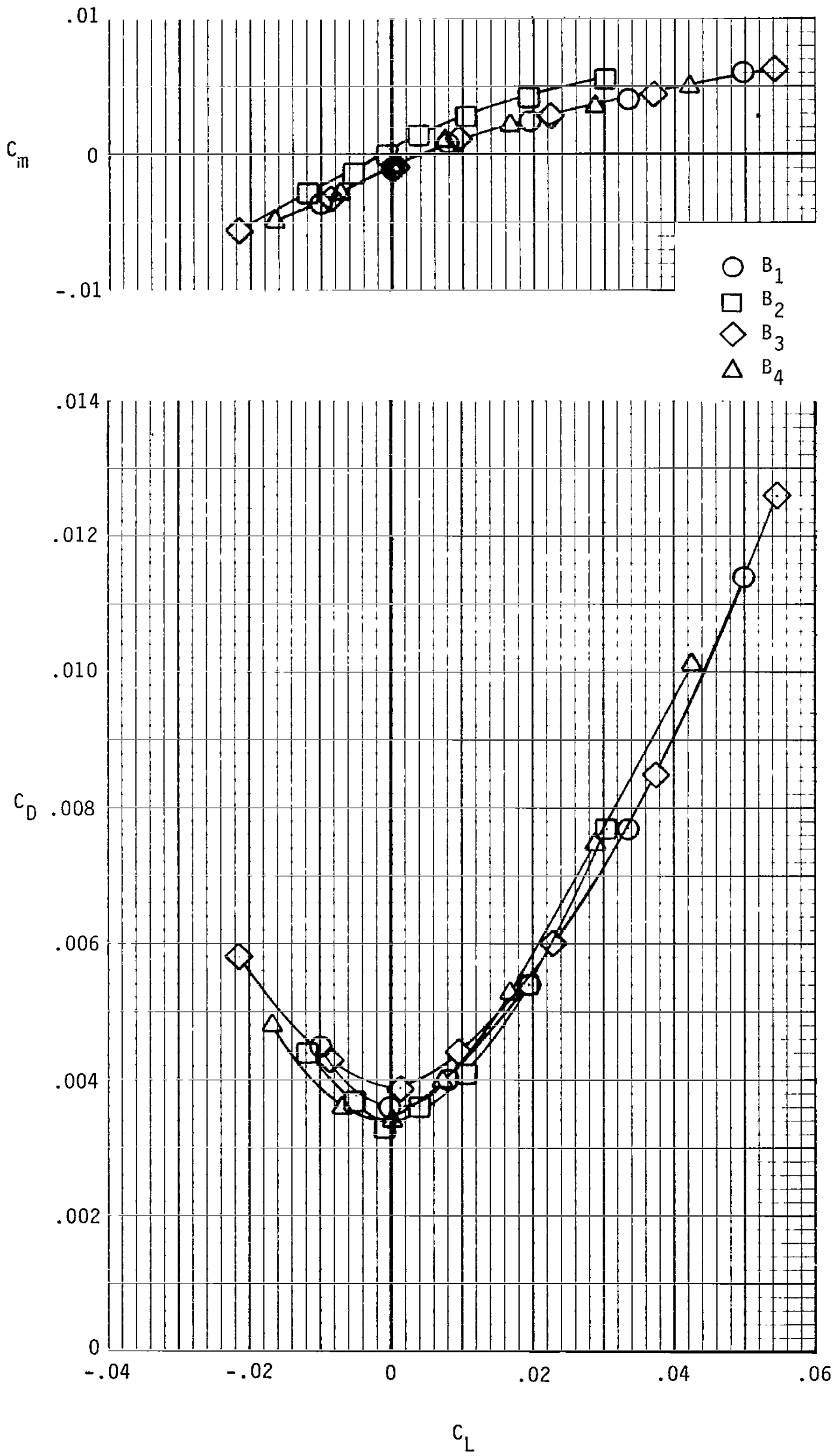

Figure 8.- Concluded.

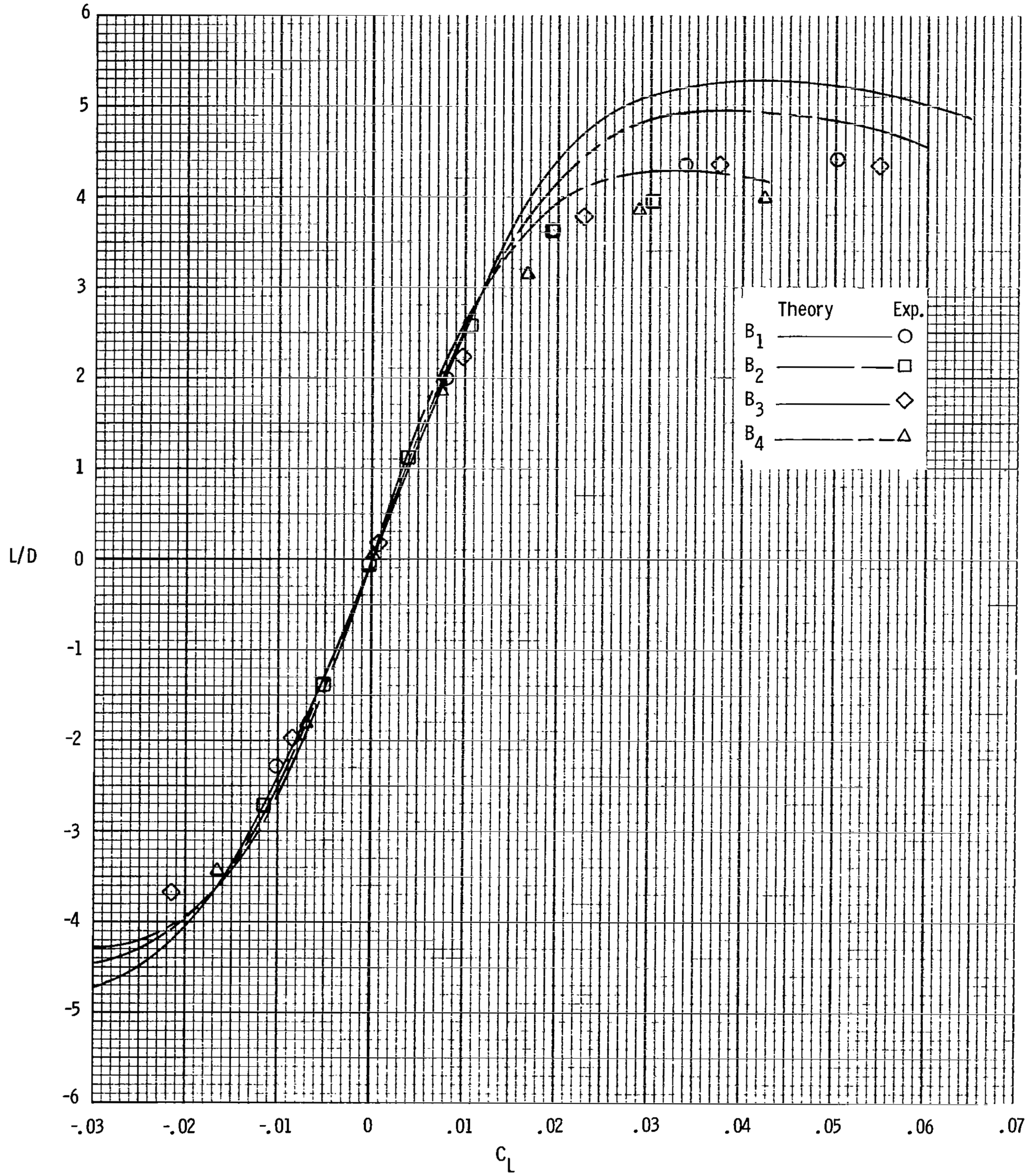

Figure 9.- Comparison of theoretical and experimental aerodynamic characteristics of four body-alone configurations.

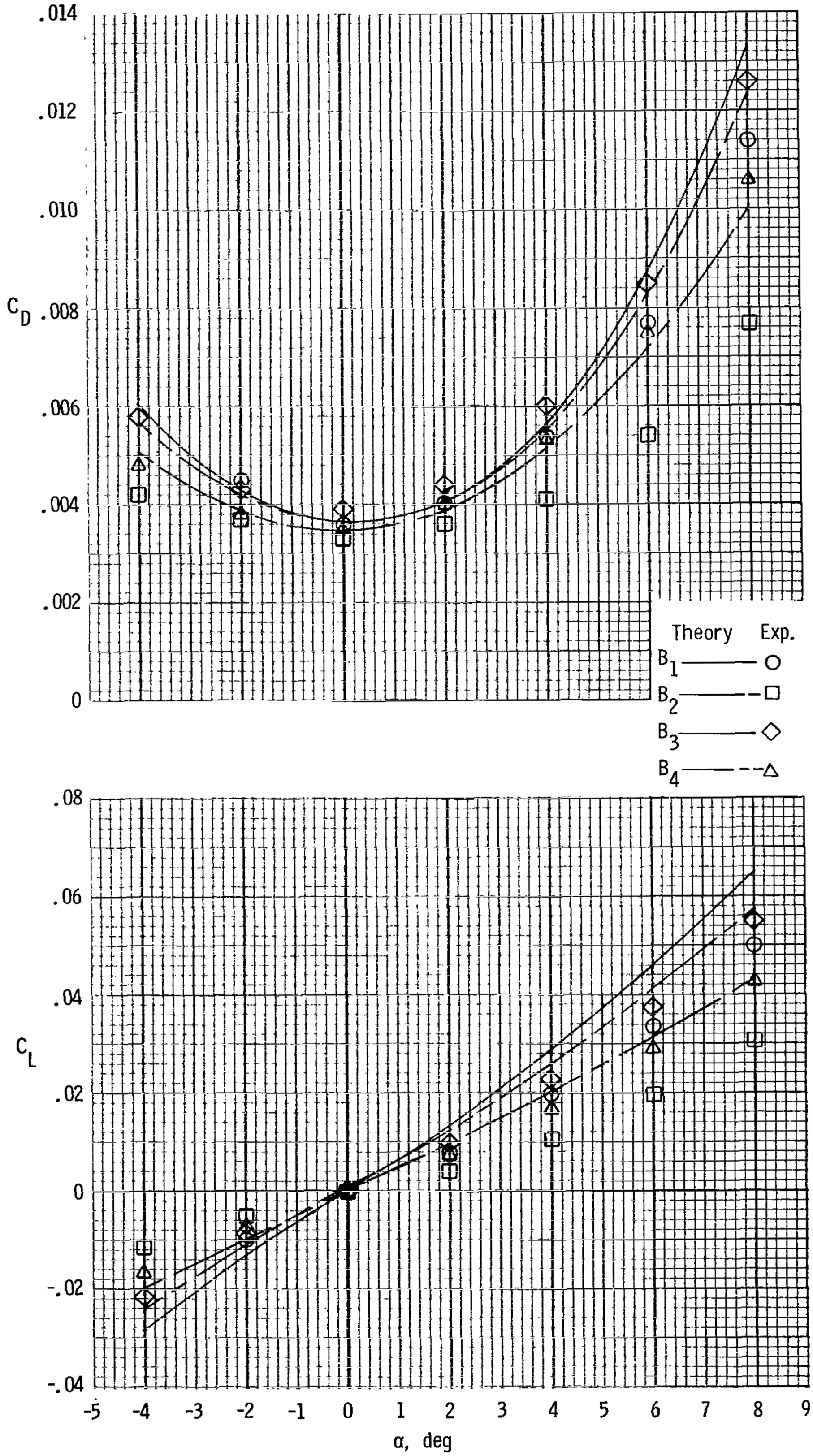

Figure 9.- Concluded.

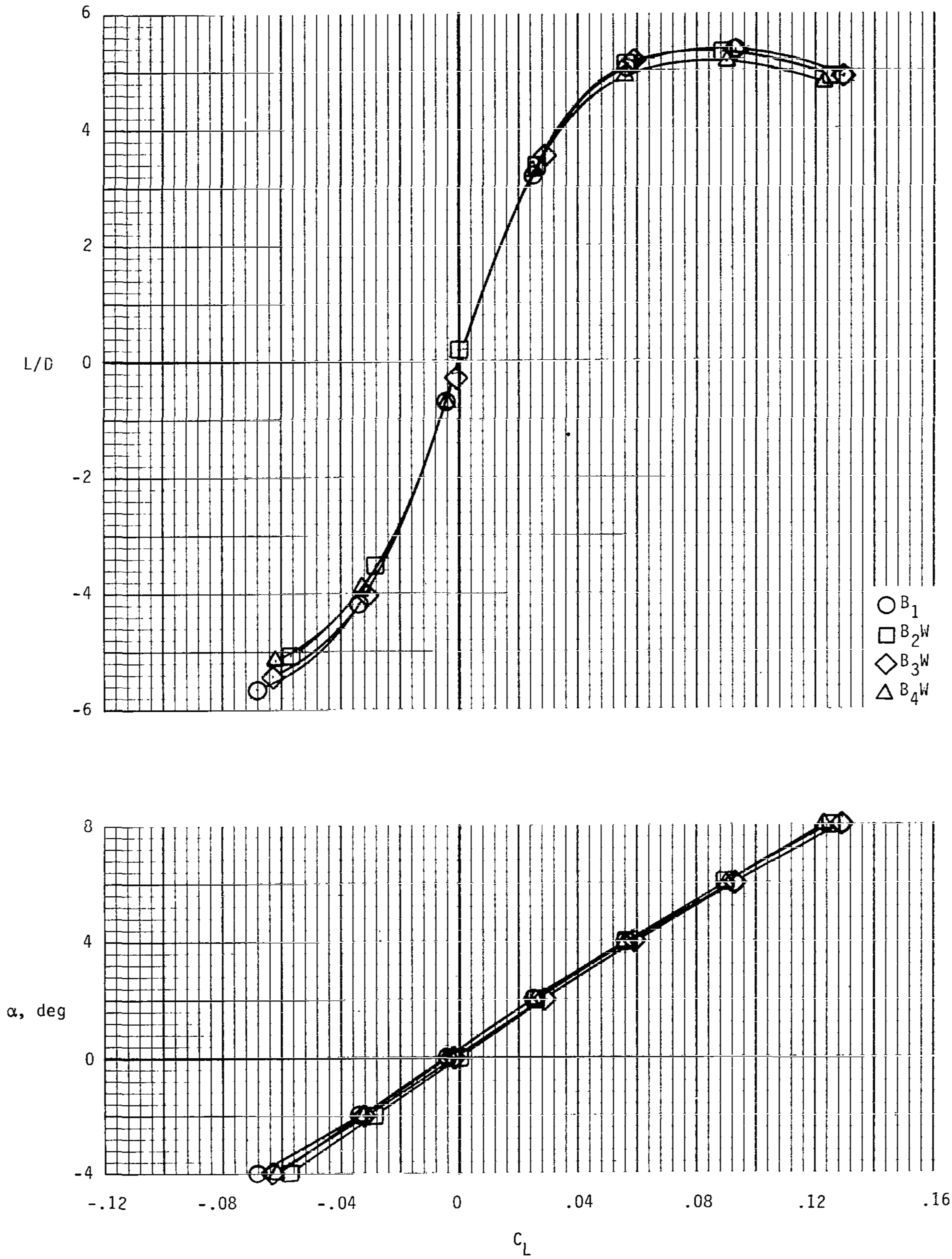

Figure 10.- Comparison of longitudinal aerodynamic characteristics of four BW configurations.

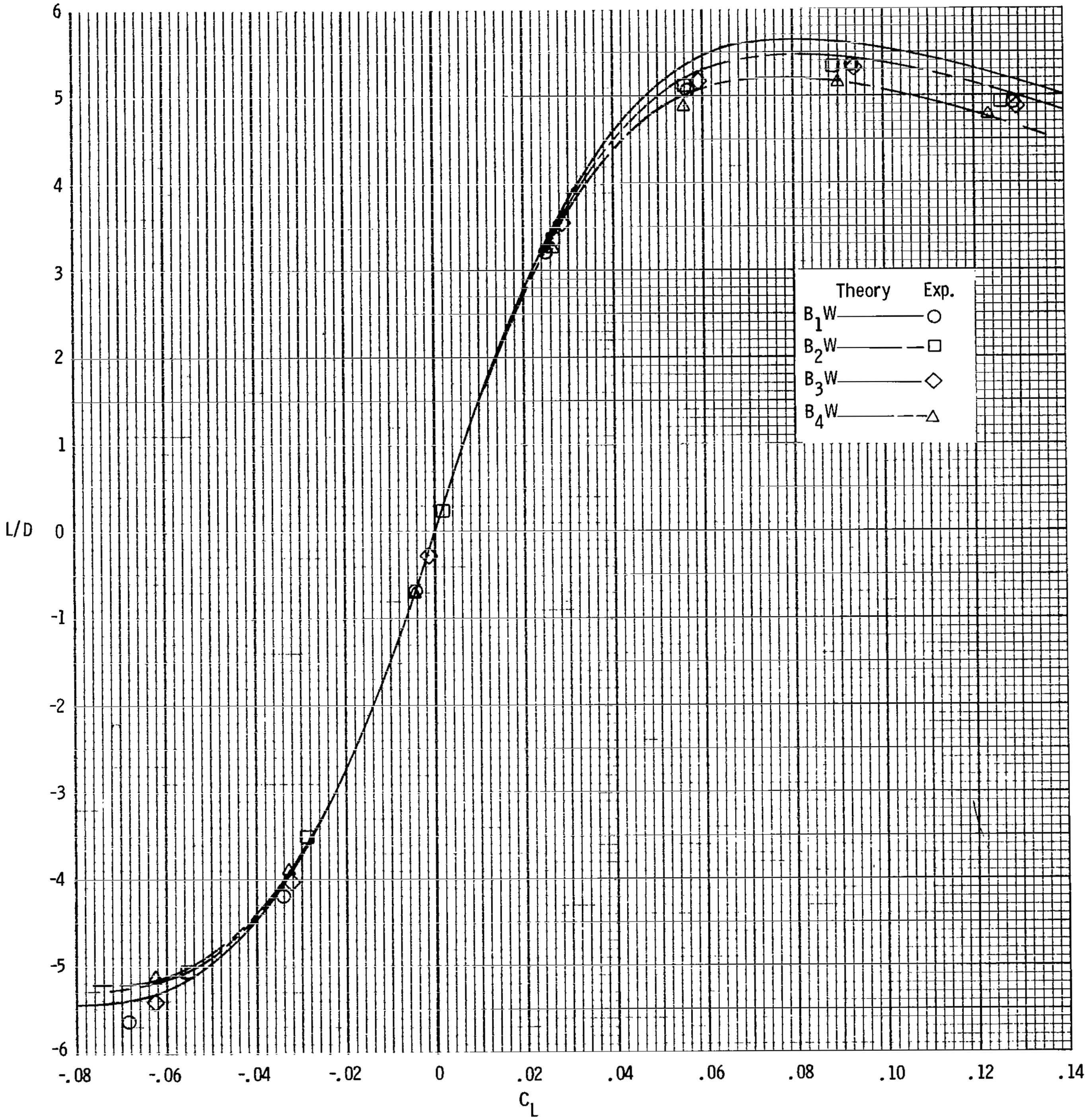

Figure 11.- Comparison of theoretical and experimental lift-drag ratios of four BW configurations.

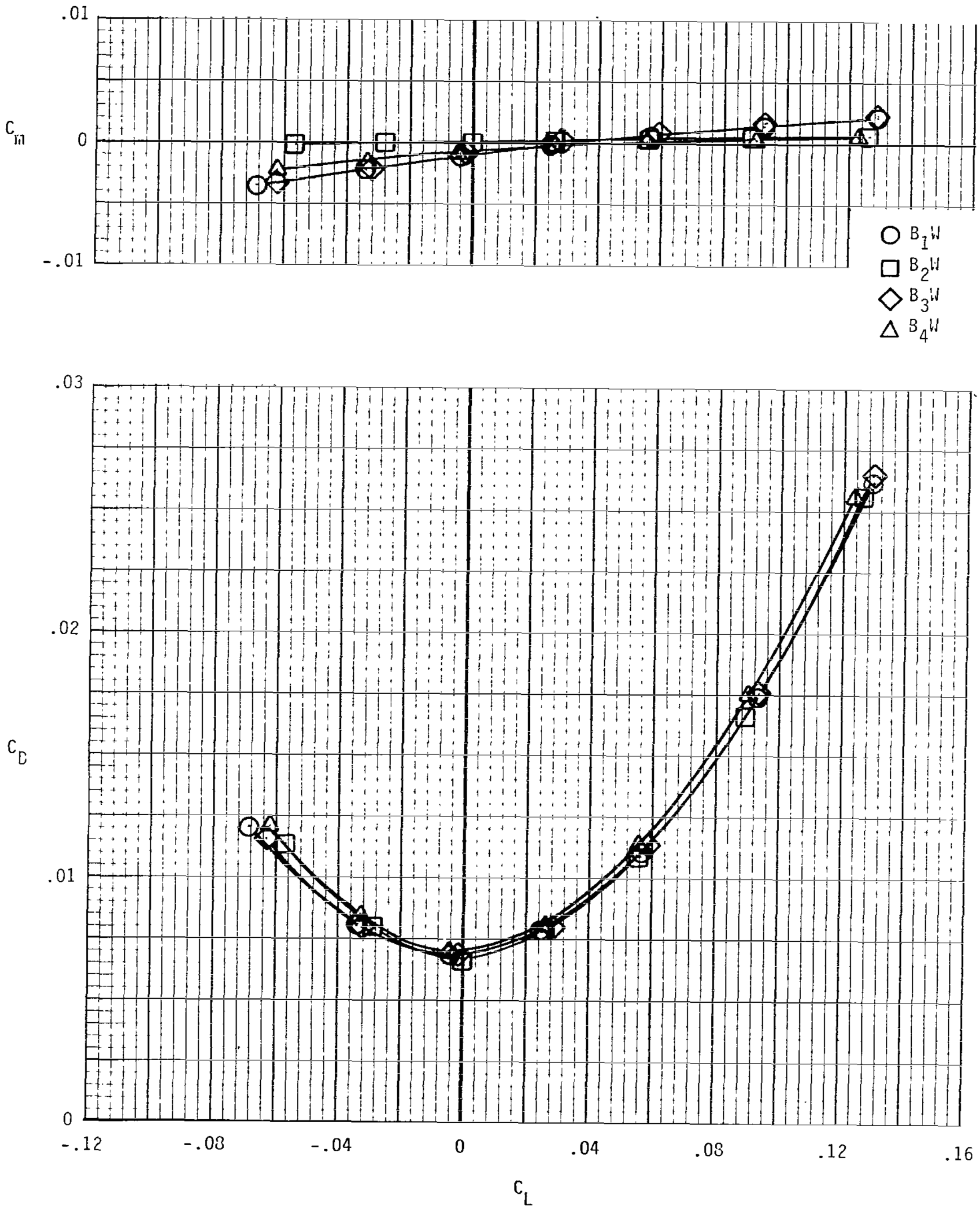

Figure 10.- Concluded.

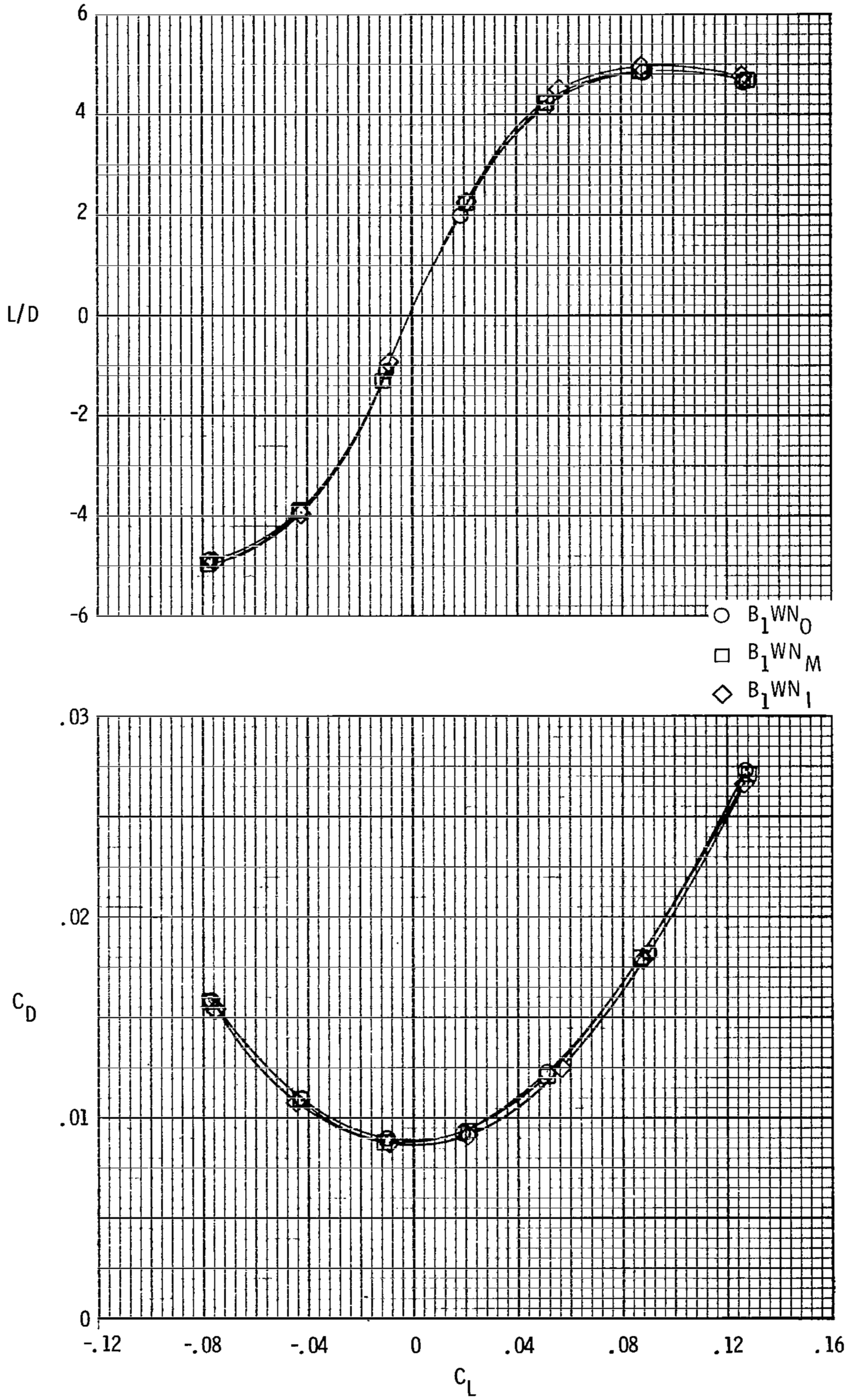

Figure 12.- Experimental aerodynamic characteristics for three nacelle positions.

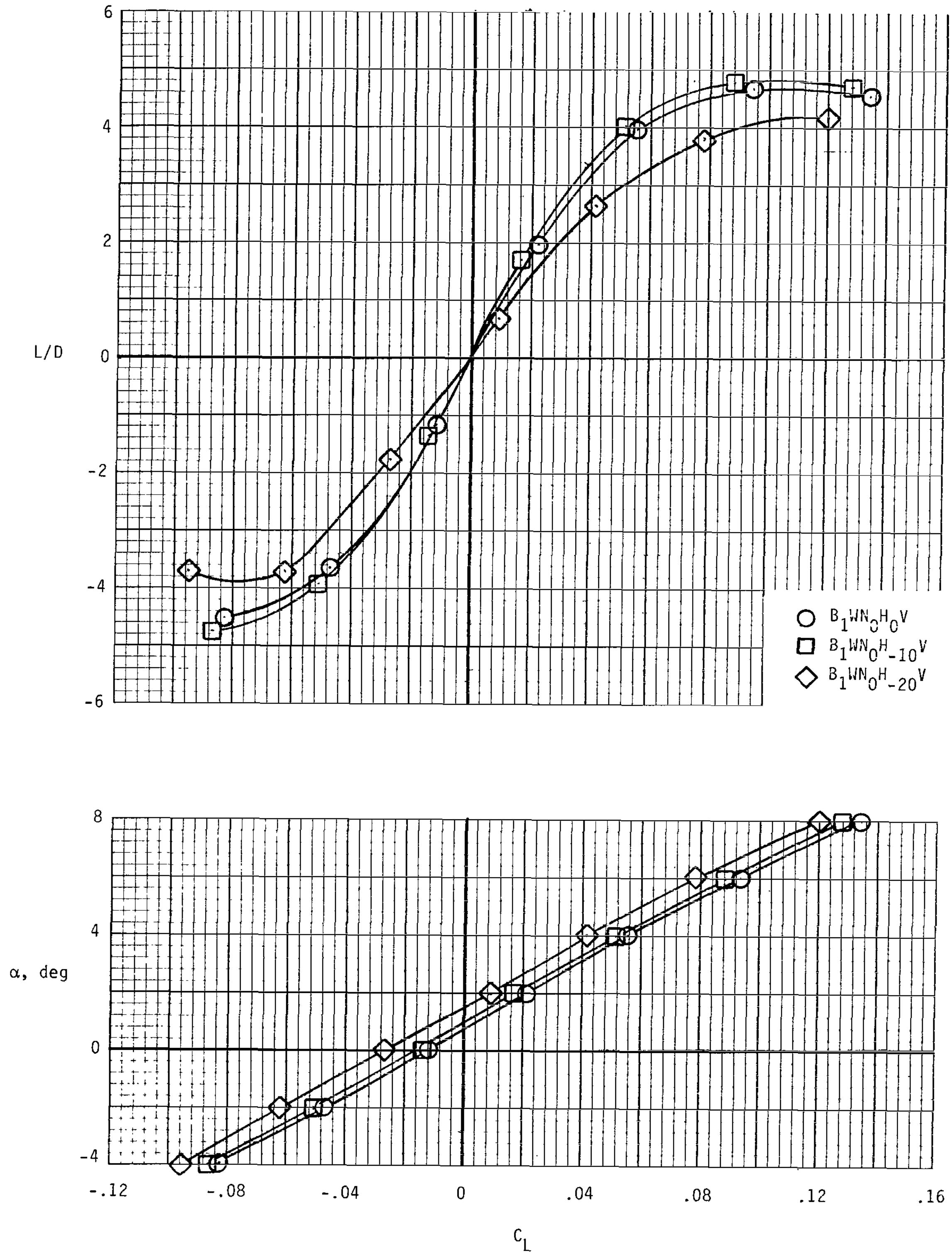

Figure 13.- Effect of horizontal tail deflection on longitudinal aerodynamic characteristics of B_1WN_0HV configuration.

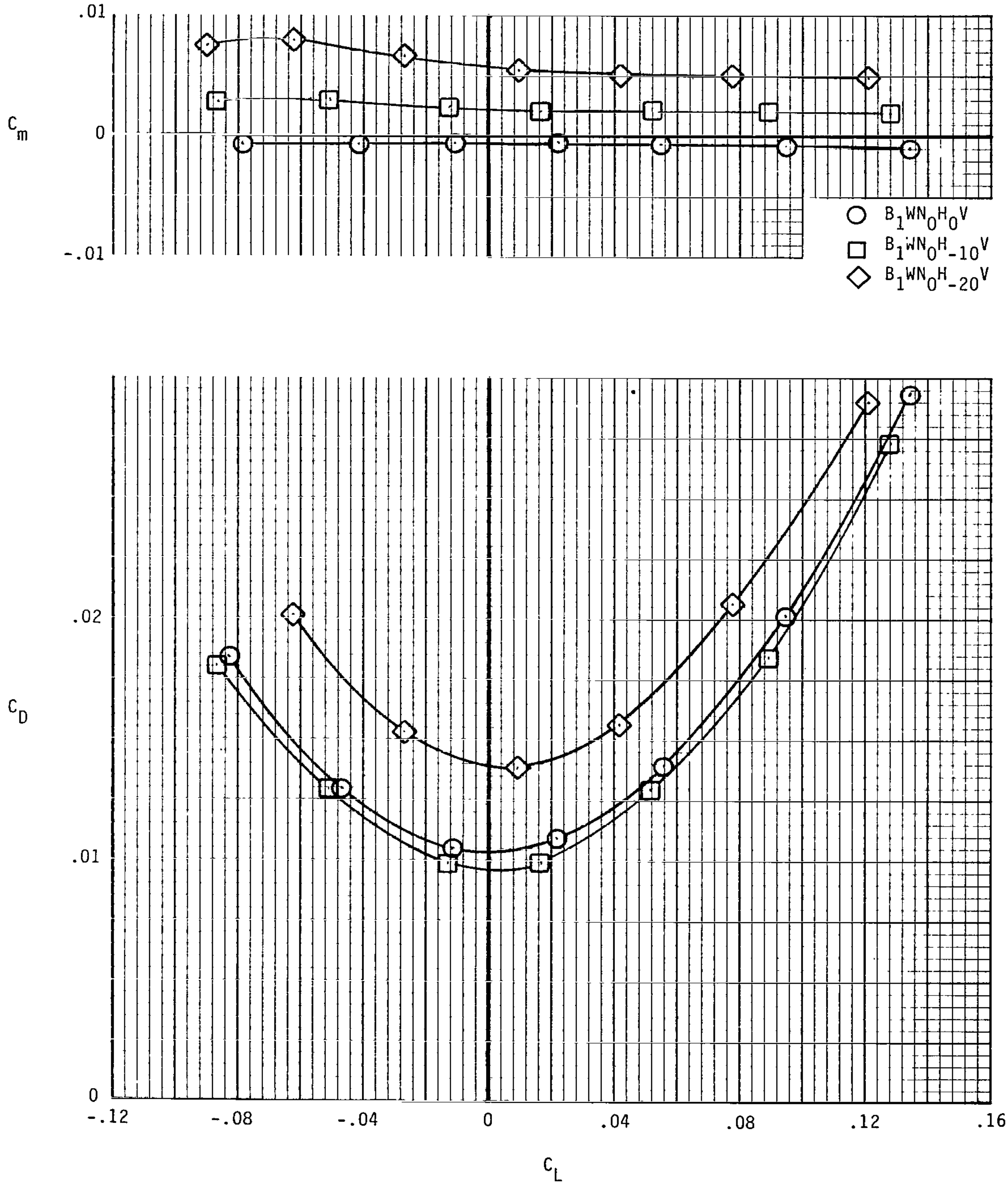

Figure 13.- Concluded.

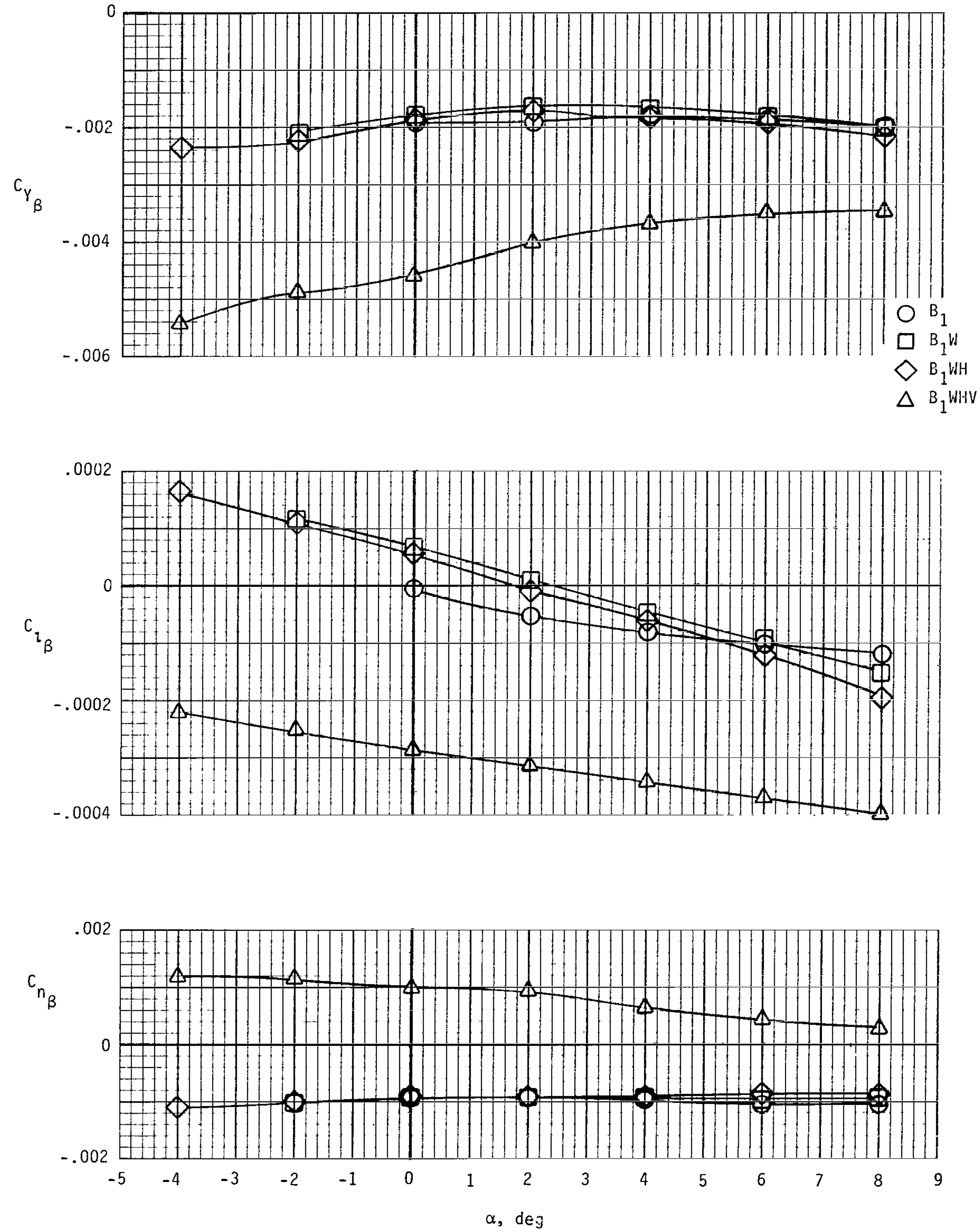

Figure 14.- Lateral-directional characteristics for B_1 configuration buildup.

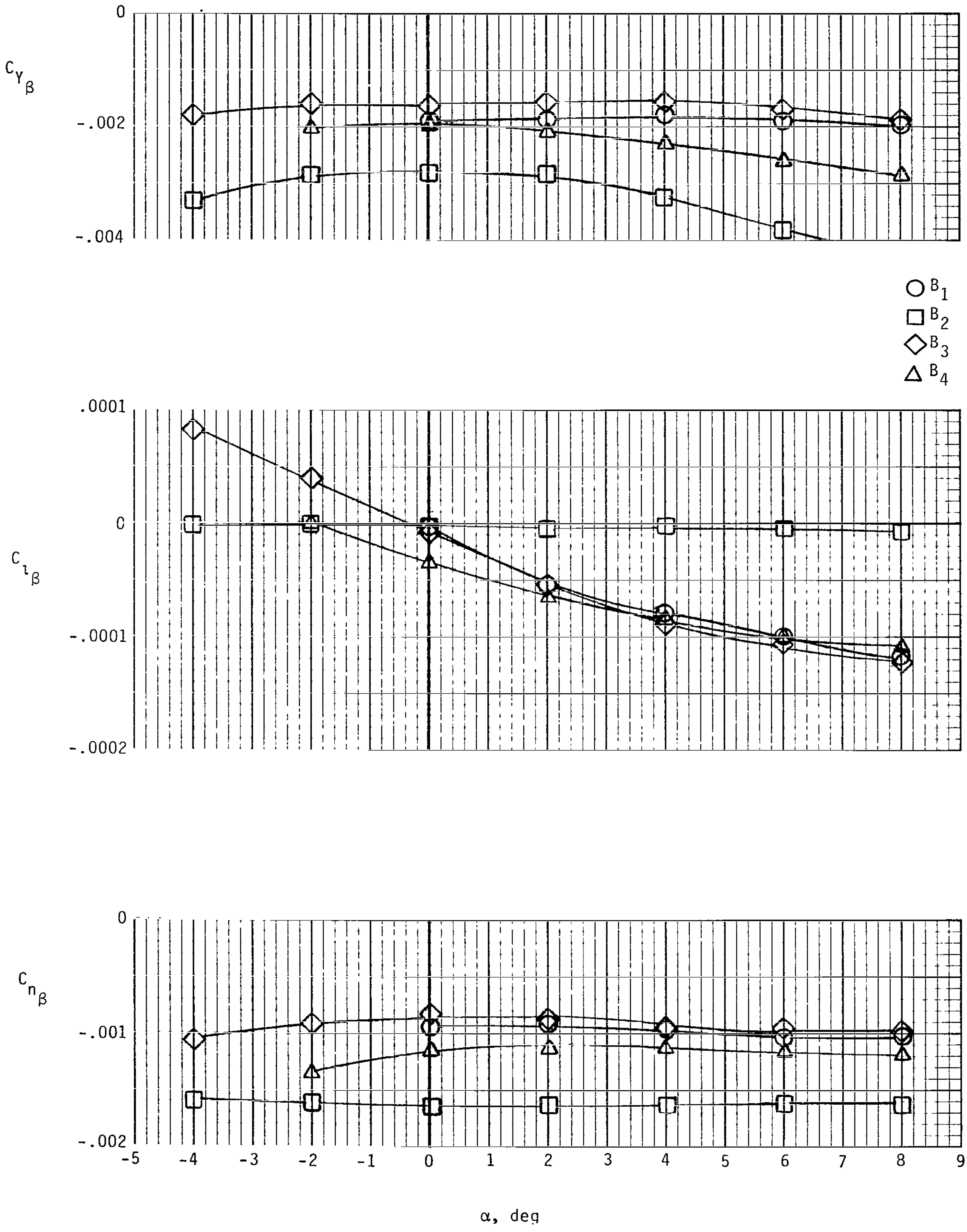

Figure 15.- Comparison of lateral-directional characteristics of body-alone configurations.

1. Report No.	2. Government Accession No.	3. Recipient's Catalog No.
NASA TP-2235		

4. Title and Subtitle
AERODYNAMIC CHARACTERISTICS, INCLUDING EFFECT OF BODY SHAPE, OF A MACH 6 AIRCRAFT CONCEPT

5. Report Date
December 1983

6. Performing Organization Code
505-43-23-10

7. Author(s)
Gregory D. Riebe

8. Performing Organization Report No.
L-15675

9. Performing Organization Name and Address
NASA Langley Research Center
Hampton, VA 23665

10. Work Unit No.

11. Contract or Grant No.

12. Sponsoring Agency Name and Address
National Aeronautics and Space Administration
Washington, DC 20546

13. Type of Report and Period Covered
Technical Paper

14. Sponsoring Agency Code

15. Supplementary Notes

16. Abstract

Longitudinal aerodynamic characteristics for a hydrogen-fueled hypersonic transport concept at Mach 6 are presented in this report. The model components consist of four bodies with identical longitudinal area distributions but different cross-sectional shapes and widths, a wing, horizontal and vertical tails, and a set of wing-mounted nacelles simulated by solid bodies on the wing upper surface. Lift-drag ratios were found to be only slightly affected by fuselage planform width or cross-sectional shape. Relative distribution of fuselage volume above and below the wing was found to have an effect on the lift-drag ratio, with a higher lift-drag ratio produced by the higher wing position.

17. Key Words (Suggested by Author(s))
Hypersonic aircraft
Body shape

18. Distribution Statement
Unclassified - Unlimited

Subject Category 02

19. Security Classif. (of this report)	20. Security Classif. (of this page)	21. No. of Pages	22. Price
Unclassified	Unclassified	30	A03

For sale by the National Technical Information Service, Springfield, Virginia 22161

NASA-Langley, 1983